PHYSICAL REVIEW B **89**, 081104(R) (2014)

$J_{\text{eff}} = \frac{1}{2}$ Mott spin-orbit insulating state close to the cubic limit in Ca_4IrO_6

S. Calder,[1,*] G.-X. Cao,[2,3] S. Okamoto,[3] J. W. Kim,[4] V. R. Cooper,[3] Z. Gai,[5] B. C. Sales,[3] M. D. Lumsden,[1] D. Mandrus,[2,3] and A. D. Christianson[1]

[1]*Quantum Condensed Matter Division, Oak Ridge National Laboratory, Oak Ridge, Tennessee 37831, USA*
[2]*Department of Materials Science and Engineering, University of Tennessee, Knoxville, Tennessee 37996, USA*
[3]*Materials Science and Technology Division, Oak Ridge National Laboratory, Oak Ridge, Tennessee 37831, USA*
[4]*Advanced Photon Source, Argonne National Laboratory, Argonne, Illinois 60439, USA*
[5]*Center for Nanophase Materials Sciences, Oak Ridge National Laboratory, Oak Ridge, Tennessee 37830, USA*

(Received 12 June 2013; revised manuscript received 20 January 2014; published 10 February 2014)

The $J_{\text{eff}} = \frac{1}{2}$ state is manifested in systems with large cubic crystal field splitting and spin-orbit coupling that are comparable to the on-site Coulomb interaction, U. $5d$ transition-metal oxides host parameters in this regime and strong evidence for this state in Sr_2IrO_4, and additional iridates, has been presented. All the candidates, however, deviate from the cubic crystal field required to provide an unmixed canonical $J_{\text{eff}} = \frac{1}{2}$ state, impacting the development of a robust model of this novel insulating and magnetic state. We present experimental and theoretical results that not only show Ca_4IrO_6 hosts the state, but furthermore uniquely resides in the limit required for a canonical unmixed $J_{\text{eff}} = \frac{1}{2}$ state.

DOI: 10.1103/PhysRevB.89.081104 PACS number(s): 75.70.Tj, 71.20.Be, 71.20.Ps, 78.70.Nx

The competition between spin-orbit coupling (SOC), on-site Coulomb interaction and crystalline electric field (CEF) splitting in certain $5d$ iridates results in an electronic configuration that supports a novel $J_{\text{eff}} = \frac{1}{2}$ Mott spin-orbit insulating state [1]. This state has been observed in Sr_2IrO_4 (Sr-214) [1], $Sr_3Ir_2O_7$ (Sr-327) [2,3], Ba_2IrO_4 (Ba-214) [4], $CaIrO_3$ [5], $BaIrO_3$ [6], and Na_2IrO_3 [7] and has been shown to remain upon dilution of the Ir ion site with, for example, Mn substitution in Sr-214 [8]. Common to all candidate $J_{\text{eff}} = \frac{1}{2}$ materials is the coexistence of magnetic order within the insulating state, with the state remaining robust in alternative magnetic structures. Similarities to the high-T_c superconducting cuprates in Sr-214 have added an extra dimension of interest [9]. Open questions, however, have emerged regarding the role of crystal symmetry, SOC, and magnetism, as well as debate over whether unequivocal experimental evidence of the $J_{\text{eff}} = \frac{1}{2}$ state exists [10–12].

The $J_{\text{eff}} = \frac{1}{2}$ state requires local cubic symmetry resulting in isotropic CEF splitting, in addition to appreciably strong SOC [13]. Significantly all proposed $J_{\text{eff}} = \frac{1}{2}$ candidates, however, deviate from the cubic limit resulting in a mixed $J_{\text{eff}} = \frac{1}{2}, \frac{3}{2}$ ground state. For example, in Sr-214 the octahedra are elongated by ∼4% along the c axis resulting in tetragonal corrections to the ground state [14]. A consideration of Sr_3CuIrO_6, with a noncubic deviation of the O-Ir-O octahedral angle from 90° to 80°, proposed that the result was a mixing away from a pure $J_{\text{eff}} = \frac{1}{2}$ ground state due to the anisotropic CEF splitting [15]. Additionally, debate has emerged as to what role, if any, the magnetic order that occurs in the insulating phase plays. Indeed there have been suggestions that rather than a Mott insulating state, which necessitates a Coulomb driven opening of the band gap, a magnetically driven opening of the band gap via the Slater mechanism plays a crucial role [16]. Finding a material with properties within the cubic limit is an important step required to aid the building of a robust model of the insulating and magnetic state in $J_{\text{eff}} = \frac{1}{2}$ iridates.

We consider such a candidate material, Ca_4IrO_6 (space group $R\bar{3}c$), an insulator at room temperature that contains Ir^{4+} ions, as found in previous $J_{\text{eff}} = \frac{1}{2}$ insulators [17–19]. Initial investigations of Ca_4IrO_6 considered the Ir ions as residing on quasi-one-dimensional spin chains on a frustrated lattice [18], a topology that could be expected to suppress long range magnetic order. Subsequent specific heat and susceptibility measurements [19,20] and a recent μSR investigation [21], however, indicated the onset of magnetic correlations around 12 K. In Ca_4IrO_6 the IrO_6 octahedra are well separated and disconnected, with no shared Ir-O-Ir bonds between octahedra. The octahedra contain identical Ir-O bond lengths, with a deviation of the O-Ir-O angle of $<2°$ from 90°. Subsequently the IrO_6 octahedral environment in Ca_4IrO_6 resides close to the ideal cubic-atomic limit required for the CEF and SOC splitting of the d manifold to produce an unmixed $J_{\text{eff}} = \frac{1}{2}$ ground state. We present neutron, resonant x-ray scattering (RXS), and density functional theory (DFT) results that support this postulate and additionally report the development of long range magnetic order.

Single crystals of Ca_4IrO_6 with dimensions 0.1 mm^3 were grown using the flux method. 4 g of powder Ca_4IrO_6 was prepared using solid-state techniques. Neutron scattering was performed on the powder sample at the High Flux Isotope Reactor using the triple axis instruments HB-3 and HB-1A in elastic mode with a wavelength of 2.36 Å and on the powder diffractometer HB-2A with wavelength 1.54 Å. An annular aluminum sample holder was utilized to reduce neutron absorption. Single crystal measurements were performed using magnetic RXS at the Advanced Photon Source on beamline 6-ID-B at both the L_2 (12.83 keV) and L_3 (11.22 keV) resonant edges of iridium. Graphite was used as the polarization analyzer at the (0 0 10) and (008) reflections on the L_2 and L_3 edges, respectively, to achieve a scattering angle close to 90°. We performed polarization analysis of the photon beam in σ-π and σ-σ mode to separate out the magnetic and charge scattering, respectively. To observe the sample fluorescence, energy scans were performed without the analyzer and with the detector away from any Bragg peaks through both absorption

*caldersa@ornl.gov

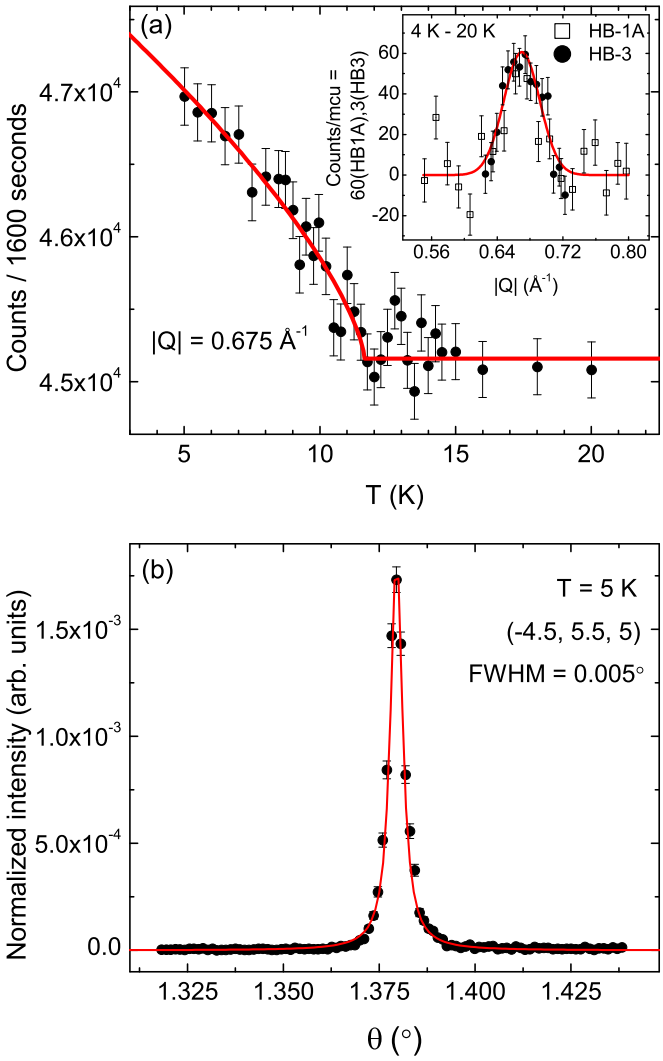

FIG. 1. (Color online) (a) Elastic neutron diffraction on beamlines HB-3 and HB-1A around $|Q| = 0.67$ Å^{-1}. (Inset) 4 K minus 20 K data. The results are scaled to account for the different neutron flux on each instrument. (Main panel) Intensity measured at $|Q| = 0.67$ Å^{-1} using HB-3 showing the onset of magnetic ordering around 12 K. (b) RXS measurement of the magnetic (−4.5,5.5,5) reflection of Ca_4IrO_6 at the L_3 resonant edge (11.215 keV) in σ-π mode.

energies. The DFT calculations were performed with the generalized gradient approximation and projector augmented wave (PAW) approach [22] as implemented in the Vienna *ab initio* simulation package (VASP) [23,24], with relativistic SOC included. The experimental structure in Ref. [19] was used with a $2 \times 2 \times 2$ k-point grid, doubled unit cell and an energy cutoff of 550 eV. We employ the rotationally invariant LDA + U method of Liechtenstein [25] with $U = 2$ and $J = 0.2$ eV for the Ir d states, values consistent with the literature [16,26]. For Ir and O, we use standard potentials (Ir and O in the VASP distribution), and for Ca, we use PAW potentials in which semicore s and p states are treated as valence states (Capv).

We begin our investigation with a consideration of the magnetic ordering in Ca_4IrO_6, having first ruled out any thermal structural anomalies through a neutron powder diffraction investigation. Low $|Q|$ neutron measurements (see Fig. 1) show increased scattering intensity, indicative of magnetic order, at $|Q| = 0.67$ Å^{-1} in going from 20 to 4 K. The scattering is commensurate with the nuclear structure, but at a noninteger wave vector, making it compatible with antiferromagnetic ordering. Measurements on both HB-3 and HB-1A suggested a magnetic reflection at $|Q| = 1.17$ Å^{-1}, as indicated by increased intensity below 12 K. The intensity variation of the scattering at $|Q| = 0.67$ Å^{-1} with temperature is consistent with a second-order transition, as shown in Fig. 1. Fitting the results to a power law gives a transition temperature of 12 K.

To explore the ordered magnetic structure we performed a representational analysis [27]. The propagation vector $\mathbf{k} = (\frac{1}{2}\frac{1}{2}0)$ produces magnetic reflections at both $|Q| = 0.67$ Å^{-1} and $|Q| = 1.17$ Å^{-1} and no other low angle positions, consistent with the neutron data, and as we show, single crystal x-ray data. Alternative propagation vectors were considered, but all failed to give intensity at $|Q| = 0.67$ Å^{-1}. The space group $R\bar{3}c$ and Ir ions on the 6b Wyckoff position give the irreducible representations (IR) Γ_1 and Γ_3 (following the numbering scheme of Kareps). We employ the simplification for a second-order transition that only one IR describes the magnetic structure [28]. Our neutron results alone do not allow a unique determination of the magnetic structure.

RXS was performed on a single crystal of Ca_4IrO_6 with a tight mosaic ($\sim 0.005°$) (see Fig. 1). We surveyed a large number of reflections and performed a polarization analysis to confirm the magnetic or nonmagnetic nature of each reflection, observing 30 magnetic reflections. All magnetic peaks were consistent with the $\mathbf{k} = (\frac{1}{2}\frac{1}{2}0)$ propagation vector. The predicted intensity contributed from each basis vector within the two symmetry permitted IRs allows the possible moment directions to be considered. For Γ_1 (Γ_3) with moments in the ab plane only even (odd) L reflections are allowed; conversely for moments along the c axis only odd (even) L reflections are allowed. We observed both even and odd L reflections indicating the spins are not confined to either the ab plane or the c axis, independent of whether the magnetic structure is described by Γ_1 or Γ_3. This spin direction constraint produces the same allowed reflections for both Γ_1 and Γ_3.

To allow for a distinction between the two candidate magnetic structures, we performed DFT calculations using VASP. Starting with the spins in the a-c plane in both Γ_1 and Γ_3 configurations, the spins were unconstrained and stable magnetic solutions were obtained for both cases, shown in Fig. 2. We note that this is distinct from the case with the spins confined to the a-b plane, where stable magnetic solutions could only be obtained by applying extra constraints and fixing the spins. For Γ_1, the direction of magnetic moments rotated from the a-c plane to the b-c plane with the original symmetry. For both candidate magnetic structures the spins were initially not aligned along the Ir-O bond directions in the octahedra, however, they relaxed along the Ir-O directions to form the lowest energy ground state. This is similar to the behavior observed in Sr-214, where the octahedral rotation controls the spin directions and may be a general feature of magnetically ordered $J_{\text{eff}} = \frac{1}{2}$ iridates [14]. For Ca_4IrO_6 the Γ_1 magnetic structure is lower in energy, compared to the Γ_3 magnetic structure, by ~ 0.018 eV/unit cell, ~ 0.0015 eV/site. With

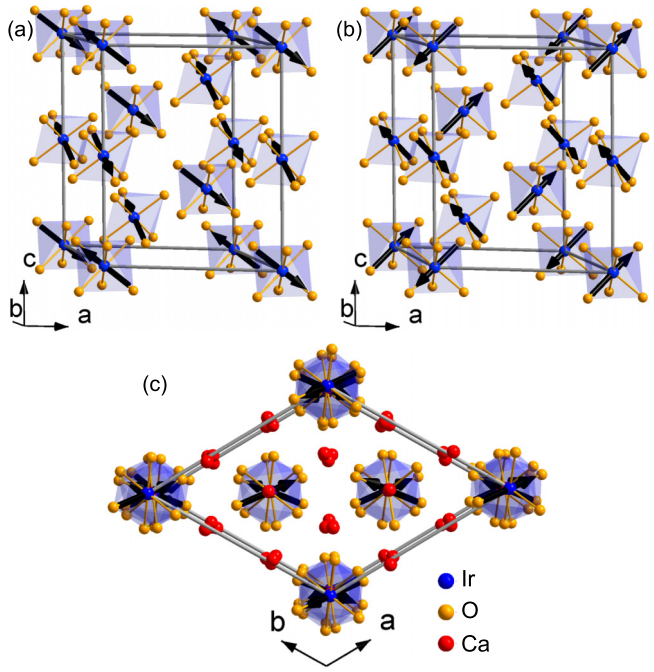

FIG. 2. (Color online) Candidate magnetic structures for Ca_4IrO_6 for the (a) Γ_1 and (b) Γ_3 IRs based on experimental results and DFT calculations. Only the nuclear unit cell is shown, with $a = 9.3$ Å, $c = 11.2$ Å. The magnetic unit cell is doubled in the a-b plane. The lowest energy magnetic structures have the spin directions along the Ir-O bond in the octahedra. (c) a-b plane view of the Γ_1 magnetic structure showing the separated IrO_6 octahedra.

$T_N = 12$ K this is an appreciably different energy scale. We therefore conclude that Γ_1, with the spins aligned as shown in Fig. 2(a), is the most likely long ranged magnetic structure for Ca_4IrO_6. Applying our DFT results for the magnetic structure to the experimental neutron data, and normalizing the intensity with respect to the nuclear reflections, gives an ordered magnetic moment of $0.42(10)\mu_B$. This value corresponds to, within experimental error, the ordered moments for the $J_{\text{eff}} = \frac{1}{2}$ materials Sr-214 [$0.208(3)$–$0.36(6)\mu_B$] [29,30], Sr-327 [$0.35(6)\mu_B$] [31], and Mn-doped Sr-214 [$0.5(1)\mu_B$] [8] found from neutron investigations.

We now turn to the insulating state of Ca_4IrO_6 by first considering DFT calculations, shown in Fig. 3. The results

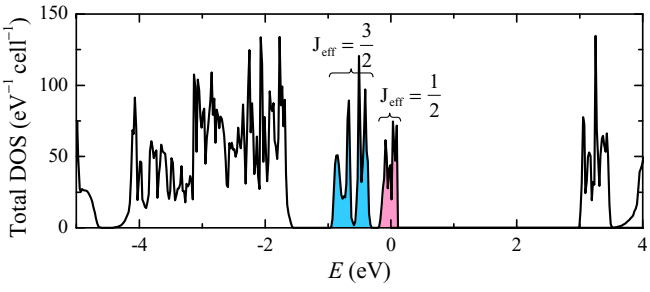

FIG. 3. (Color online) Total density of states (DOS) of Ca_4IrO_6 for the nonmagnetic case, with the inclusion of SOC and U, shows an unmixed $J_{\text{eff}} = \frac{1}{2}$ ground state.

reveal the SOC and CEF in Ca_4IrO_6 breaks the t_{2g} manifold degeneracy into $J_{\text{eff}} = \frac{1}{2}$ and $J_{\text{eff}} = \frac{3}{2}$ states. The $J_{\text{eff}} = \frac{1}{2}$ bandwidth in Ca_4IrO_6 ($\sim$0.2 eV) is much narrower than that in Sr_2IrO_4 ($\sim$1 eV) and coupled with the cubic environment results in an unmixed $J_{\text{eff}} = \frac{1}{2}$ ground state. We will return to the significance of the unmixed ground state after considering our experimental results below. A moderate U is expected to induce a Mott insulating state once one goes beyond the DFT + U calculations, for example, DFT + DMFT. For DFT + U the introduction of magnetic order splits the $J_{\text{eff}} = \frac{1}{2}$ band, resulting in insulating states with a gap amplitude around 0.6 eV for both Γ_1 and Γ_3 structures.

Experimentally, a comparison of the intensity enhancement at the L_2 and L_3 edges in RXS measurements has been shown to uncover a signature of the $J_{\text{eff}} = \frac{1}{2}$ state, initially in Sr-214 and then subsequently in Sr-327, Ba-214, and $CaIrO_3$ [1,3–5]. Specifically, for a $10Dq$ CEF split d manifold in the limit of negligible SOC splitting for Ir^{4+}, i.e., the case of $S = 1/2$, the t_{2g} manifold with both $J = 3/2$ and $J = 5/2$ is the lowest unoccupied state. Consequently both the L_2-edge ($2p_{1/2} \rightarrow 5d_{3/2}$) and L_3-edge ($2p_{3/2} \rightarrow 5d_{3/2,5/2}$) RXS transitions are allowed and appreciable intensity is expected at both edges during a measurement. Conversely for large SOC and CEF splitting, i.e., the $J_{\text{eff}} = \frac{1}{2}$ case, the $J_{\text{eff}} = \frac{3}{2}$ band in Ir^{4+} produced from the $J = 3/2$ states will be fully occupied forbidding a transition at the L_2 edge, resulting in no measured RXS intensity. Measurements at the magnetic reflection $(-0.5, 3.5, 8)$ through both L_2 and L_3 resonant energies in Ca_4IrO_6 are shown in Fig. 4(a). A large enhancement is observed at the L_3 edge that has its maximum at the inflection point of the fluorescence scans, as expected. Conversely there is no appreciable resonant enhancement at the L_2 energy, with the fluorescence scan showing a maximum at the expected L_2 edge energy. Following the methodology in Refs. [1–5] this is direct evidence for a $J_{\text{eff}} = \frac{1}{2}$ state in Ca_4IrO_6. Recently Ref. [32] argued for Sr-214 and Ba-214 the crystal symmetry coupled with spins in the ab plane could lead to a suppressed intensity at the L_2 edge irrespective of a $J_{\text{eff}} = \frac{1}{2}$ state. Consequently in those specific cases suppression of intensity at the L_2 edge is suggested to be a requirement, but not a proof of a $J_{\text{eff}} = \frac{1}{2}$ state. We note this does not apply to either the crystal or magnetic symmetry of Ca_4IrO_6, however, for robustness we have presented both experimental and theoretical verification of a $J_{\text{eff}} = \frac{1}{2}$ state.

All previous candidate $J_{\text{eff}} = \frac{1}{2}$ materials diverge from a local cubic IrO_6 environment. Such deviations have been suggested to be manifested in the ratio of the resonant intensity I_{L2}/I_{L3} [2,14]. The ideal cubic case yields an unmixed $J_{\text{eff}} = \frac{1}{2}$ state and subsequently the I_{L2}/I_{L3} ratio should be identically zero. Previous RXS investigations of $J_{\text{eff}} = \frac{1}{2}$ materials Sr-214, Sr-327, and Ba-214 have involved Ir octahedra with axial distortions, quantified by a tetragonal splitting variable Δ. Consequently a factor θ, where $\tan(2\theta) = 2\sqrt{2}\lambda/(\lambda - 2\Delta)$, with λ the SOC, has been introduced to parametrize the tetragonal distortion with SOC and account for observed deviations from the ideal I_{L2}/I_{L3} ratio [14]. $\Delta = 0$ for Ca_4IrO_6 and as reported in Ref. [2] this should be manifested experimentally in $I_{L2}/I_{L3} = 0$ and theoretically both a symmetric spin-density profile map and a well

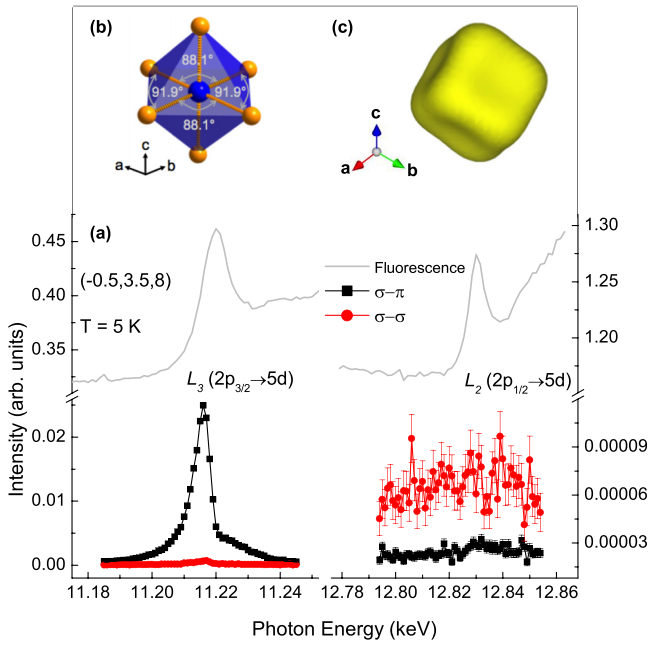

FIG. 4. (Color online) (a) RXS energy scans through the L_3 (11.22 keV) and L_2 (12.83 keV) Ir edges at the $(-0.5,3.5,8)$ magnetic reflection in Ca_4IrO_6. A large resonant enhancement occurs at L_3, whereas the intensity is suppressed at the L_2 energy. This behavior has been reported to be a signature of the $J_{\text{eff}} = \frac{1}{2}$ state. (b) Local environment of the Ir ions probed by RXS; the IrO_6 environment deviates by $<2\%$ from the ideal case. (c) Total charge density plot around an Ir ion in Ca_4IrO_6 shows a highly symmetric charge distribution.

separated $J_{\text{eff}} = \frac{1}{2}$ band. Experimentally for Ca_4IrO_6 we find no appreciable intensity at the L_2 edge, consistent with isotropic CEF splitting and strong SOC creating an unmixed $J_{\text{eff}} = \frac{1}{2}$ ground state [33]. Furthermore DFT calculations of the total charge density around the Ir ion, including SOC, show local cubic symmetry as evidenced by the dimpled dice shape in Fig. 4(c) drawn using VESTA [34]. The total DOS in Fig. 3 reveals well separated $J_{\text{eff}} = \frac{1}{2}$ and $J_{\text{eff}} = \frac{3}{2}$ bands due both to the cubic nature and well separated octahedra. Therefore the electronic structure of Ca_4IrO_6 shows the expected behavior of a material with local cubic CEF and strong SOC resulting in an unmixed $J_{\text{eff}} = \frac{1}{2}$ ground state.

Considering the magnetic and insulating states in Ca_4IrO_6 reveals two well separated phases, with $T_N = 12$ K and $T_{MIT} > 300$ K. While debate exists in Sr-214 as to whether the magnetically driven Slater mechanism plays a significant role in creating a band gap and driving the insulating state [16], the large separation between the insulating state suggests a purely Mott insulating state in Ca_4IrO_6. Furthermore we determined Ca_4IrO_6 shows a reduced ordered moment that falls within the regime of previous candidates, indicating a reduced moment is an intrinsic property of the $J_{\text{eff}} = \frac{1}{2}$ state and not a consequence of lattice distortions. Indeed, in general, the realization of an unmixed $J_{\text{eff}} = \frac{1}{2}$ state in this material will allow specific properties to be assigned, without recourse to perturbative models.

Our experimental and theoretical results have shown that Ca_4IrO_6 is a new canonical $J_{\text{eff}} = \frac{1}{2}$ Mott spin-orbit insulator, with long range magnetic order separated from the MIT, but directly coupled to the octahedra topology. Previous candidate materials have fallen outside the limit of cubic crystal field splitting and large SOC, resulting in a mixing away from a $J_{\text{eff}} = \frac{1}{2}$ ground state. This has impacted the development of a robust theory and resulted in debate as to whether previous candidate materials, such as Sr-214, deviate significantly from the J_{eff} model. Ca_4IrO_6 is a realization of a material that fills this significant gap and contains an unmixed $J_{\text{eff}} = \frac{1}{2}$ ground state. Consequently it can act as a model system to both investigate the underlying physical properties that emerge due to this novel state and reexamine previous candidates in a new light.

This research at ORNL's High Flux Isotope Reactor was sponsored by the Scientific User Facilities Division, Office of Basic Energy Sciences, US Department of Energy. Part of the work (D.M., B.C.S., G.C., V.R.C., and S.O.) was supported by the Department of Energy, Basic Energy Sciences, Materials Sciences and Engineering Division. Use of the Advanced Photon Source, an Office of Science User Facility operated for the US DOE Office of Science by Argonne National Laboratory, was supported by the US DOE under Contract No. DE-AC02-06CH11357.

[1] B. J. Kim, H. Ohsumi, T. Komesu, S. Sakai, T. Morita, H. Takagi, and T. Arima, Science **323**, 1329 (2009).

[2] J. W. Kim, Y. Choi, J. Kim, J. F. Mitchell, G. Jackeli, M. Daghofer, J. van den Brink, G. Khaliullin, and B. J. Kim, Phys. Rev. Lett. **109**, 037204 (2012).

[3] S. Boseggia, R. Springell, H. C. Walker, A. T. Boothroyd, D. Prabhakaran, D. Wermeille, L. Bouchenoire, S. P. Collins, and D. F. McMorrow, Phys. Rev. B **85**, 184432 (2012).

[4] S. Boseggia, R. Springell, H. C. Walker, H. M. Rønnow, C. Rüegg, H. Okabe, M. Isobe, R. S. Perry, S. P. Collins, and D. F. McMorrow, Phys. Rev. Lett. **110**, 117207 (2013).

[5] K. Ohgushi, J.-i. Yamaura, H. Ohsumi, K. Sugimoto, S. Takeshita, A. Tokuda, H. Takagi, M. Takata, and T.-h. Arima, Phys. Rev. Lett. **110**, 217212 (2013).

[6] M. A. Laguna-Marco, D. Haskel, N. Souza-Neto, J. C. Lang, V. V. Krishnamurthy, S. Chikara, G. Cao, and M. van Veenendaal, Phys. Rev. Lett. **105**, 216407 (2010).

[7] Y. Singh, S. Manni, J. Reuther, T. Berlijn, R. Thomale, W. Ku, S. Trebst, and P. Gegenwart, Phys. Rev. Lett. **108**, 127203 (2012).

[8] S. Calder, G.-X. Cao, M. D. Lumsden, J. W. Kim, Z. Gai, B. C. Sales, D. Mandrus, and A. D. Christianson, Phys. Rev. B **86**, 220403(R) (2012).

[9] J. Kim, D. Casa, M. H. Upton, T. Gog, Y.-J. Kim, J. F. Mitchell, M. van Veenendaal, M. Daghofer, J. van den Brink, G. Khaliullin, and B. J. Kim, Phys. Rev. Lett. **108**, 177003 (2012).

[10] L. C. Chapon and S. W. Lovesey, J. Phys.: Condens. Matter **23**, 252201 (2011).

[11] S. Fujiyama, H. Ohsumi, K. Ohashi, D. Hirai, B. J. Kim, T. Arima, M. Takata, and H. Takagi, Phys. Rev. Lett. **112**, 016405 (2014).
[12] H. Zhang, K. Haule, and D. Vanderbilt, Phys. Rev. Lett. **111**, 246402 (2013).
[13] A. Abragam and B. Bleaney, *Electron Paramagnetic Resonance of Transition Ions* (Clarendon, Oxford, 1970).
[14] G. Jackeli and G. Khaliullin, Phys. Rev. Lett. **102**, 017205 (2009).
[15] X. Liu, V. M. Katukuri, L. Hozoi, W.-G. Yin, M. P. M. Dean, M. H. Upton, J. Kim, D. Casa, A. Said, T. Gog, T. F. Qi, G. Cao, A. M. Tsvelik, J. van den Brink, and J. P. Hill, Phys. Rev. Lett. **109**, 157401 (2012).
[16] R. Arita, J. Kuneš, A. V. Kozhevnikov, A. G. Eguiluz, and M. Imada, Phys. Rev. Lett. **108**, 086403 (2012).
[17] R. F. Sarkozy, C. W. Moeller, and B. L. Chamberland, J. Solid State Chem. **9**, 242 (1974).
[18] M. J. Davis, M. D. Smith, and H.-C. z. Loye, Acta Crystallogr., Sect. C: Cryst. Struct. Commun. **57**, 1234 (2001).
[19] N. Segal, J. F. Vente, T. S. Bush, and P. D. Battle, J. Mater. Chem. **6**, 395 (1996).
[20] G. Cao, V. Durairaj, S. Chikara, S. Parkin, and P. Schlottmann, Phys. Rev. B **75**, 134402 (2007).
[21] I. Franke, P. J. Baker, S. J. Blundell, T. Lancaster, W. Hayes, F. L. Pratt, and G. Cao, Phys. Rev. B **83**, 094416 (2011).
[22] P. E. Blöchl, Phys. Rev. B **50**, 17953 (1994).
[23] G. Kresse and J. Furthmüller, Phys. Rev. B **54**, 11169 (1996).
[24] G. Kresse and D. Joubert, Phys. Rev. B **59**, 1758 (1999).
[25] A. I. Liechtenstein, V. I. Anisimov, and J. Zaanen, Phys. Rev. B **52**, R5467 (1995).
[26] B. J. Kim, H. Jin, S. J. Moon, J.-Y. Kim, B.-G. Park, C. S. Leem, J. Yu, T. W. Noh, C. Kim, S.-J. Oh, J.-H. Park, V. Durairaj, G. Cao, and E. Rotenberg, Phys. Rev. Lett. **101**, 076402 (2008).
[27] A. S. Wills, Physica B **276**, 680 (2000).
[28] We treat the magnetic transition in Ca_4IrO_6 as continuous based on our experimental results and previous measurements in the literature in Refs. [20, 21]. The ratio of the number of symmetry operations through the transition $N(G_0)/n(G_k) = 3$, this may indicate a weakly first-order transition [35].
[29] C. Dhital, T. Hogan, Z. Yamani, C. de la Cruz, X. Chen, S. Khadka, Z. Ren, and S. D. Wilson, Phys. Rev. B **87**, 144405 (2013).
[30] F. Ye, S. Chi, B. C. Chakoumakos, J. A. Fernandez-Baca, T. Qi, and G. Cao, Phys. Rev. B **87**, 140406 (2013).
[31] C. Dhital, S. Khadka, Z. Yamani, C. de la Cruz, T. C. Hogan, S. M. Disseler, M. Pokharel, K. C. Lukas, W. Tian, C. P. Opeil, Z. Wang, and S. D. Wilson, Phys. Rev. B **86**, 100401 (2012).
[32] M. Moretti Sala, S. Boseggia, D. F. McMorrow, and G. Monaco, Phys. Rev. Lett. **112**, 026403 (2014).
[33] To quantify this difference in intensity we find a ratio $I_{L2}/I_{L3} = 3.2(6) \times 10^{-4}$ for Ca_4IrO_6. We considered the resonant edge intensities from previous published candidate materials to obtain estimates of I_{L2}/I_{L3} values, while noting the difficulty in quantitatively comparing different experiments and materials using RXS. We find from Ref. [1] Sr-214 has a ratio of 4.3×10^{-2} and for Sr-327 ratios of 9.6×10^{-3} and 1.4×10^{-2} from Refs. [2, 3].
[34] K. Momma and F. Izumi, J. Appl. Crystallogr. **41**, 0653 (2008).
[35] A. Cracknell, *Magnetism in Crystalline Materials* (Pergamon Press, Oxford, 1975), p. 88.